THE JOURNAL OF PHYSICAL CHEMISTRY C

Article

pubs.acs.org/JPCC

Optical Determination of Silicon Nanowire Diameters for Intracellular Applications

John F. Zimmerman,[†] Graeme F. Murray,[†] and Bozhi Tian*[,†,‡,§]

[†]Department of Chemistry, University of Chicago, Chicago, Illinois 60637, United States

[‡]The Institute for Biophysical Dynamics, University of Chicago, Chicago, Illinois 60637, United States

[§]The James Franck Institute, University of Chicago, Chicago, Illinois 60637, United States

Supporting Information

ABSTRACT: Silicon nanowires (SiNWs) are an important class of materials for biomedical and electronics applications, with the nanowire diameter playing a fundamental role in device functionality. Here we present a method, based on light scattering intensity and ensemble electron microcopy (EM) measurements, that allows for a precise optical determination of a specific NW's diameter within an accuracy of a few nanometers (4.8 nm), an error of only ∼8.0%. This method takes advantage of the strong dependence of optical scattering on SiNW diameter to construct an optical to EM transform, with Lorentz-Mie theory showing that this method can be used for NWs up to ∼150 nm in diameter. Additionally, this technique offers some potential insights into biophysical interactions, allowing the optical calibration of individual intracellular SiNW force probes, enabling a ∼100-fold improvement in experimental uncertainty. Using these probes, we were able to measure drug-induced vasoconstriction in human aortic smooth muscle cells (HASMCs), which exerted ∼171 pN of force after ∼30 min of exposure to the hormone angiotension II. These findings represent a scalable method for characterizing SiNW-based devices that are easily extendable to other materials and could be of use in ensuring quality control for future photovoltaics, optical sensors, and nanomaterial biosensors.

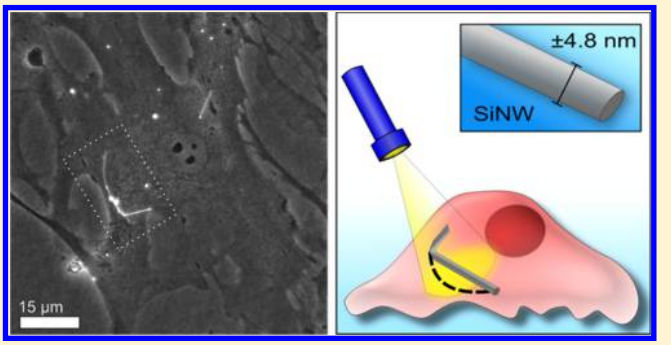

1. INTRODUCTION

The optical properties of semiconducting silicon nanomaterials have drawn much interest recently, as these structures can display interesting size-dependent optical properties both on the ensemble level,[1−3] and at the single nanowire scale,[4] with such materials being considered for applications in photovoltaic devices,[5−9] wave guides,[5,10] colorimetric markers[11] and photodetectors.[5,12,13] One critical aspect of these materials is their characteristic nanometer-sized diameters, which can play an important role in governing device performance and affects such properties as charge distribution,[14] temperature sensitivity,[15] and photovoltaic quantum efficiency.[16] Therefore, a precise determination of nanowire diameter is important for many device applications, and could be of potential interest as part of the quality control process for consumer products.

Previous work has shown that the diameter of nanowires can be determined optically using the nanowire's dark field (DF) spectra,[17,18] and has even been used for in situ monitoring of nanowire growth.[19] To achieve this, an in-optics spectrometer is required, which can collect the optical spectrum of individual nanowires; however, these setups can be expensive and are not commonly available in most laboratories. Additionally, the requirement for an optical spectrum can limit access to in situ biological applications, as only certain spectral windows are available in tissue and media samples,[20] preventing the collection of a complete spectrum. However, recent work has been done on integrating nanowires with biological systems,[21] for instance as next generation biosensors[22,23] and drug delivery vectors.[24] Therefore, a more ideal system would be able to observe both cellular components and silicon nanomaterials simultaneously, while remaining readily achievable at the laboratory scale. To demonstrate that such a system is possible, here we show that optical scattering intensity is strongly correlated with silicon nanowire (SiNW) diameter. Using ensemble information about the sample's optical scattering intensity and underlying the diameter population (collected using electron microscopy, EM), we are able to construct an optical-EM transform which allows for the precise determination of an individual SiNW's diameter using DF microscopy (Figure 1).

Furthermore, we show that this work is relevant to the emerging field studying the bionanomaterials interface. In our previous work, we demonstrated that kinked SiNWs can be used as intracellular force probes to study cell behavior.[25] Using Euler−Bernoulli beam theory, we were able to model SiNW deformation to extract force information from the observed

Received: October 14, 2015
Revised: November 25, 2015

DOI: 10.1021/acs.jpcc.5b10076
J. Phys. Chem. C XXXX, XXX, XXX−XXX

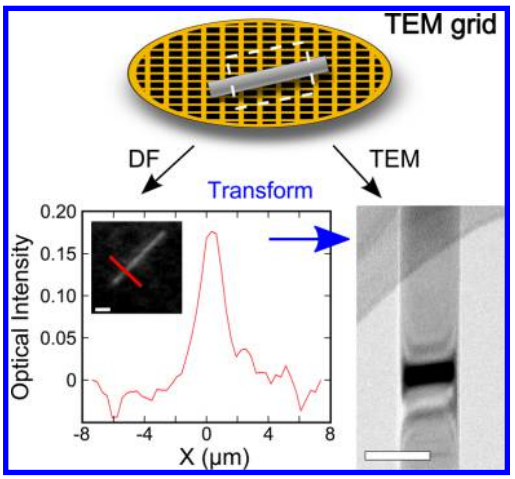

Figure 1. Schematic illustration of mapping between optical signal intensity and TEM measured SiNW diameters. The same SiNW is shown both under DF (left) and TEM (right), with the corresponding line scan taken over the highlighted region (scale bars 5 μm and 25 nm, respectively). An optical transform function would alleviate the need for individual correlative studies. To obtain the optical-EM transform, ensemble DF and TEM micrographs are used to construct a mapping function, providing an optical method to precisely determine SiNW diameters.

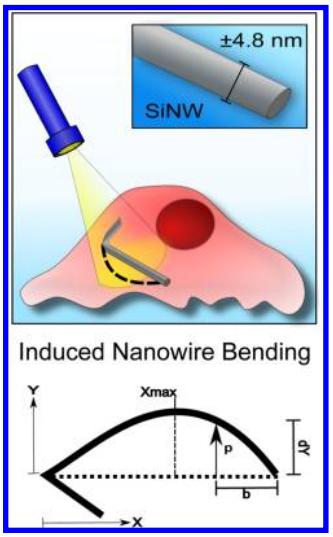

Figure 2. SiNW diameter plays a critical role in calibrating Intracellular force probes. (Upper) Schematic illustration of a kinked SiNW intracellular force probe inside a human aortic smooth muscle cell (HASMC), bending in response to intracellular forces. (Lower) Euler–Bernoulli model of a simply supported bending SiNW beam is used to measure the resulting force load, P, which scales as $P \propto D^{-4}$, where D is the SiNW diameter. This makes D a critical parameter for precisely calibrating these intracellular probes.

nanowire bending (Figure 2). However, the force loads, P, modeled this way scale as $P \propto D^{-4}$, where D is the nanowire's diameter. As a result, the absolute values of the predicted forces are very sensitive to even small changes in SiNW diameter. While this still allows for a relative measurement of the time-evolved forces experienced within a cell, it makes a precise determination of the magnitude of these forces difficult to achieve. Therefore, to calibrate this system, a careful measurement of the SiNW diameter is needed for each force probe. One way to achieve this is to fix and then stain these samples for examination under transmission electron microscopy (TEM); however, this presents several challenges. First, while much work has been recently done on correlative light-electron microscopy,[26] it can still be difficult to track individual cells across microscopes and requires a significant time investment for each sample. Second, cell fixation can lead to cellular artifacts, limiting the accuracy of these methods. Therefore, a more desirable approach to calibrate these probes would be to use an independent technique that allows for the characterization of the underlying nanomaterials, circumventing this time-consuming process. To achieve this, we have introduced a method that relies on ensemble population distributions, meaning that individual force probes can be optically calibrated, circumventing the need to use EM methods for each individual force probe.

2. EXPERIMENTAL METHODS

2.1. SiNW Synthesis. SiNWs were grown using the vapor–liquid–solid mechanism in a home-built chemical vapor deposition system. To clean the silicon growth substrates, they were first rinsed with acetone and isopropyl alcohol (IPA), and then dried under nitrogen gas. Substrates were then oxygen plasma cleaned (Plasma Etch PS-100LF) for 10 min, and coated in 1:3 dilute poly-L-lysine for 15 min. After rinsing with deionized water, gold nanoparticles between 20 and 250 nm (Ted Pella Inc.) were allowed to settle for 30 min and were then dried under nitrogen gas. SiNW growth conditions were as follows: 480 °C, 40 Torr, 60 sccm hydrogen carrier gas, and 2 sccm silane. In the case of intracellular force probes, kinks were introduced into the wires as previously reported.[27]

2.2. Correlative Optical and EM Measurements. To obtain correlative microscopy images, appropriate wires were sonicated in IPA and dropcast onto lacy carbon coated copper or gold electron microscopy grids (Electron Microscopy Sciences). TEM micrographs were obtained using a 300 kV FEI Tecnai G2 F30 Super Twin Transmission Electron Microscope. After TEM imaging, the grids were then transferred to an Olympus IX71 inverted microscope, and submerged in the appropriate optical media (i.e., air or IPA). LUCPlanFLNPh 20× and 40× objectives were used with a numerical aperture (NA) of 0.4 and 0.65 respectively. High angle transmitted darkfield micrographs were obtained using a using an Amscope LED-144-YK ring lamp LED attached to the brightfield condenser, as previously described.[25] Typical LED power was between 15%–20% of maximum power. Images were recorded on a Hamamatsu ORCA-R2 C10600-10B digital CCD camera at 16-bit depth with 0.3 × 0.3 μm^2 pixel resolution. For comparative intensity measurements, the illuminating light intensity and image exposure times were maintained across all samples.

2.3. Cell Culture. HASMCs were cultured under sterile conditions using M231 growth media (Gibco) with supplement (FBS, 4.9% v/v; fibroblast growth factor, 2 ng/mL; EGF 0.5, ng/mL; heparin, 5 ng/mL; gentamicin, 40 μg/mL; human insulin-like growth factor-I, 2 μg/mL; and BSA, 0.2 μg/mL). Cell cultures were maintained at 37 °C and under 5% CO_2, with media exchanged after 24 h, and every 48 h thereafter. All cells were between passages three to nine. Both plastic and glass substrates were used. For uptake, SiNWs were sonicated into M231 media for 1 min, and pipetted into a culture dish. SiNWs were allowed to settle overnight, before HASMCs were introduced. HASMCs were incubated with the SiNWs ≈ 72 h before vasoconstriction was introduced using the hormone

DOI: 10.1021/acs.jpcc.5b10076
J. Phys. Chem. C XXXX, XXX, XXX–XXX

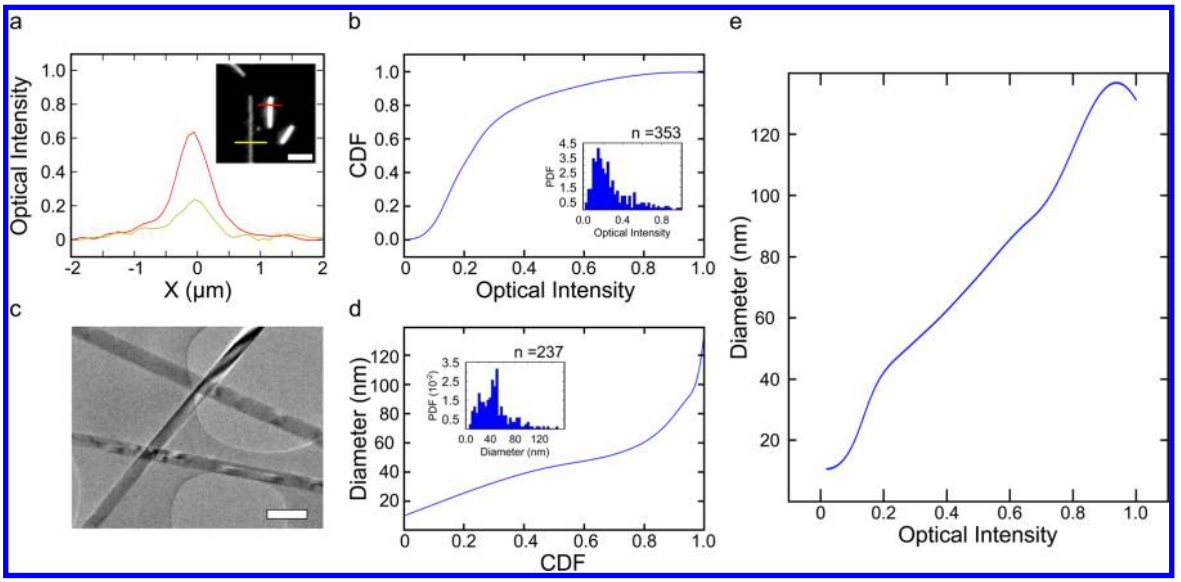

Figure 3. Constructing the Optical-EM transform. (a) Representative line scan measurement of relative SiNW optical intensities, with corresponding DF image (inset, Scale bar 4 μm) (region of line scan in yellow and red). (b) Cumulative distribution function (CDF) of ensemble SiNW optical scattering intensity, with associated population distribution (inset). (c) Representative TEM micrograph of SiNWs used to measure ensemble SiNW diameters (Scale bar 150 nm). (d) Inverse CDF of ensemble SiNW diameters as measured by TEM (upper), with associated population distribution (given as a probability density function, PDF) (inset). (e) Empirically determined optical-EM transform constructed using the ensemble CDFs. Allows the assignment of individual SiNW diameter using optical intensity data.

angiotension II human (50−75 nM, Sigma-Aldrich). For live cell optical imaging, the same optical setup as described above was used, with the addition of an INUB-ONICS-F1 Takai Hit stage top incubator, which helped maintain physiological conditions (i.e., 95% humidity, 37 °C internal temperatures, 5% CO_2).

3. RESULTS AND DISCUSSION

3.1. Constructing the Optical Transform. To optically determine the diameter of an individual SiNW with subdiffraction precision, we have constructed a nonparametric transform from optical scattering intensity to SiNW diameter, using prior ensemble electron microscopy (EM) measurements. This method makes use of cumulative distribution functions (CDF), for both optical scattering intensity and sample diameter (Figure 3). This provides an estimate for the range of possible SiNWs diameters and optical scattering intensities in a given sample preparation. By establishing this range, it is possible to determine where an individual SiNW lies within this distribution, and enables a prediction of the SiNW's diameter. In other words, this allows a conversion between relative light scattering intensities into population percentile, and then back out again into NW diameter. By using CDFs, an exact parametrization of the Optical-EM transform is not needed, but instead a statistically driven determination is possible. In general, this method yields reasonable diameter estimates for the majority of wires surveyed, providing diffraction-limited information. Additionally, by avoiding a direct parametrization certain issues like device-substrate photonic interactions, which are difficult to resolve theoretically,[28] can be incorporated into the transform.

Underlying this method is the assumption that an SiNW's scattering intensity scales monotonically with regard to NW diameter. That is to say, that as SiNWs grow in diameter, they scatter light more intensely (or at least as intensely). Without this condition, the cumulative mapping function fails to pair optical intensities correctly with their corresponding diameters. To probe this condition and obtain a theoretical understanding of the principles underlying SiNW optical scattering, we will use Lorentz-Mie theory based calculations. Lorentz-Mie theory has previously offered some insight into nanomaterials systems such as GaAs,[17] germanium,[29] and silicon nanowires,[4] and will provide a basis for understanding this underlying assumption, allowing us to establish a range over which the optical-EM transform is valid. Collectively, this approach allows us to map the optical scattering intensity of a SiNW to its diameter, enabling a subdiffraction determination of a given nanowire's diameter.

To measure ensemble SiNW optical scattering intensities, $I(\lambda)_{norm}$, wires were sonicated and drop cast onto lacy-carbon-coated copper or gold electron microscopy grids. Samples were then submerged in isopropyl alcohol (IPA) and imaged using a DF optical microscopy setup. IPA was selected as a model medium as it has a similar refractive index (RI) compared to cellular systems (RI: 1.378 and 1.402, respectively).[30] To later incorporate this method with cellular systems, DF micrographs were obtained using a ring LED illuminator, enabling the use of scatter enhanced phase contrast (SEPC) imaging (a simultaneously projected DF-phase contrast image).[25] For ensemble measurements, a single line scan was taken along the wire body (Figure 3a), with scattering intensity $I(\lambda)$ measured transverse to the long SiNW axis, allowing a measurement of both the local background $I(\lambda)_{bkg}$ and SiNW scattering $I(\lambda)_s$ intensities. Intensity measurements were normalized using the eq (Figure S1):

$$I(\lambda)_{norm} = \frac{I(\lambda)_S - I(\lambda)_{bkg}}{I(\lambda)_{s,max}} \quad (1)$$

where $I(\lambda)_{s,max}$ is the maximum observed scattering intensity for all wires within a sample population after background subtraction. To construct the optical scattering intensity CDF (Figure 3b), peak scattering intensity, $I(\lambda)_{norm}$, were recorded

DOI: 10.1021/acs.jpcc.5b10076
J. Phys. Chem. C XXXX, XXX, XXX−XXX

for a representative portion of the SiNWs, providing an optical population distribution. This allowed a transform from optical scattering intensities $I(\lambda)_{norm}$ to population percentile.

To determine the underlying SiNW diameter population, samples were imaged using transmission electron microscopy (TEM), with micrographs taken at random, predetermined locations prior to viewing to avoid biased sampling (Figure 3c). TEM provided high-resolution images of the SiNWs with an associated error of ±2.4 nm (~2.0% error), with this uncertainty arising primarily from small inconsistencies in the SiNWs surface morphology formed during the synthetic growth process, rather than imprecision in the measuring process. Collectively, these micrographs were used to measure the distribution of diameters present in the sample, and enabling the construction of the corresponding inverse CDF (Figure 3d). This allowed a mapping from population percentile into SiNW diameter. We note here that the samples measured in this way need not be the exact wires imaged under DF (in fact, this negates the point, as these wires could be imaged directly under TEM to determine their diameter), but must be wires from the same representative sample population. This enables an independent characterization of the SiNWs, allowing the wires to be optically imaged under conditions that are difficult to probe using electron microscopy, while still permitting a precise determination of the NW's diameter. In this way, this method differs from the exact transform, which would measure the same wires under both techniques, but instead depends on a statistical determination of the wire's diameter. We also note that, while TEM provides a mechanism for precisely measuring resolution-limited data, this role could be served by other methods, such as atomic force microscopy (AFM), or scanning electron microscopy (SEM), as long as the inverse CDF can be obtained.

Taken together, the optical CDF and the inverse NW diameter CDF, allow the construction of a transform from scatter intensity $I(\lambda)_{norm}$ to SiNW diameter (Figure 3e). To enable a continuous mapping, the optical CDF and the inverse NW diameter CDF were fit using a piece-wise cubic polynomial spline function (Figure S2). The resulting population-specific transform was found to be relatively linear, showing only small deviations before 40 nm and after 100 nm. To test this validity of this method, individual wires were measured using both DF and TEM techniques (Figure 4, Figure S3). The optical-EM transform was then applied to the experimentally determined optical scattering intensities to predict the SiNW diameters, which were then compared to the experimentally measured values obtained via TEM. To account for deviations in the optical intensity profile, both the mean and the mode of the optical scatter intensity $I(\lambda)_{norm}$ distribution were determined for each wire. This was achieved using a custom NIH ImageJ script, which processed iterative line scans across the length of each wire, incorporating multiple DF micrographs (Figure S4).

Comparing the TEM measured diameters to the predicted values, the optical-EM transform introduced a systematic error, which tended to on average under-predict SiNW diameters by ~8.9 nm, forecasting smaller wires than were actually present. This systematic error suggests that the optical population did not correctly reflect the underlying diameter population; specifically, smaller diameter wires were under-represented optically. This result is well explained through Lorentz-Mie scattering theory and will be discussed later in further detail. After applying this correction factor, predicted wire diameters were well correlated with experimental results (Figure 4b),

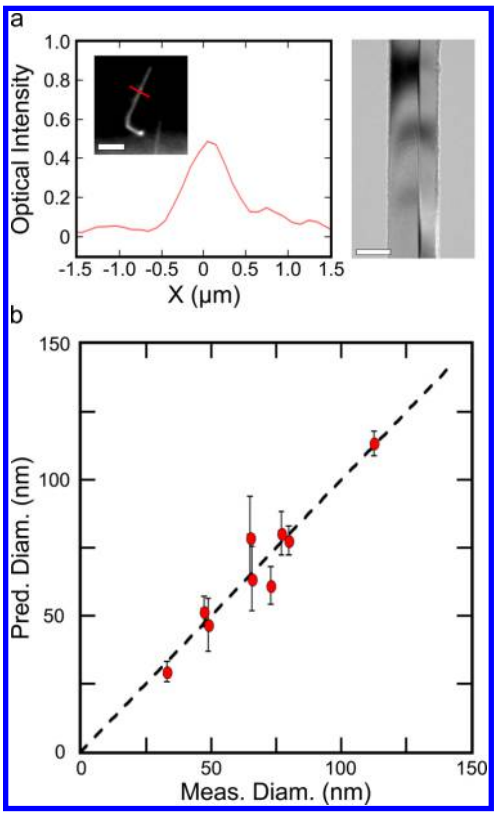

Figure 4. Verifying the Optical-EM transform. To evaluate the optical-EM transform, individual wires were evaluated, measuring their scattering intensity and diameter. (a) Example wire's scattering intensity (left) using DF (inset, Scale bar 4 μm), and diameter using TEM (right, Scale bar 50 nm). The Optical-EM transform was used to predict the SiNW diameter (predicted diameter: 77.7 nm, measured diameter: 79.8 nm). (b) Measured wire diameters compared to optically predicted diameters (unity given as dashed line, error bars given as the standard deviation of the transformed optical intensity).

showing on average only a 4.8 nm deviation from the measured values (~8.0% error in SiNW diameter). This demonstrates a predictive capability that is well below the diffraction limit, with measurements remaining reliable across a range of diameters (between ~25−125 nm). The uncertainty associated with an individual SiNW's diameter prediction was estimated using the standard deviation of the transformed optical intensity measurements (shown as error bars for Figure 4b), which proved to be a reasonable estimate as the expected population of TEM measured diameters fell within a single standard deviation of the optically predicted values. Overall this demonstrates that this method is capable of "breaking" the optical resolution limit, given some prior information about the sample population.

Before further employing this method, however, we need to consider the maximum range over which we can make reliable predictions. Furthermore, we must address the underlying assumption that scattering intensity scales monotonically with regard to nanowire diameter. To explore these topics, we have turned to Lorentz-Mie scattering theory, which offers some insights into possible experimental limitations.

3.2. Calculations of Optical Scattering using Lorentz-Mie theory. Lorentz-Mie theory offers an analytical approach to solving Maxwell's equations for passive elastic light scattering, and can be used to explore SiNW scattering behavior.[4] As the optical-EM transform uses the intensity of

DOI: 10.1021/acs.jpcc.5b10076
J. Phys. Chem. C XXXX, XXX, XXX−XXX

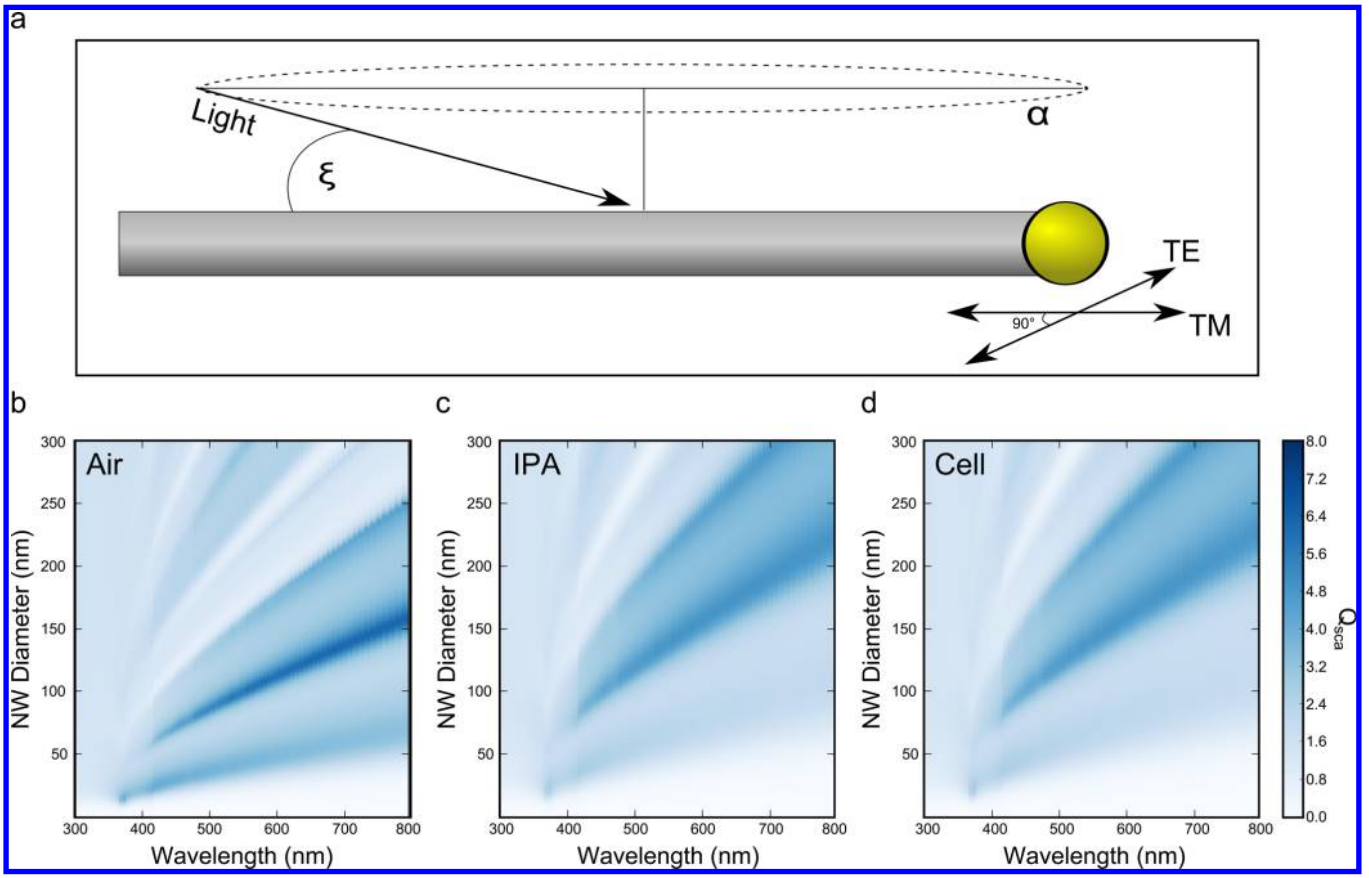

Figure 5. Mie scattering of silicon nanowires. (a) Schematic drawing of SiNW light scattering model for Mie theory calculations. Arrows indicates the incident light angle, ξ, and the corresponding plane of the TE and TM fields, with α representing the field of illumination. Calculated scattering efficiencies Q_{sca} of SiNWs for nonpolarized light at a normal ($\xi = 90°$) scattering angle in (b) air, (c) isopropyl alcohol (IPA), and (d) cytoplasm as a function of wavelength λ and SiNW diameter D.

scattered light to determine an SiNW's diameter, it is this measurement that we are most interested in. The intensity of scattered light, $(\lambda)_{norm}$, is proportional to the product of the illuminating light intensity, $S(\lambda)$, and the dimensionless unit scattering efficiencies, Q_{sca}, such that,

$$I(\lambda) \propto S(\lambda)\cdot Q_{sca}(D, \lambda) \tag{2}$$

with Q_{sca} defined as follows:

$$Q_{sca}(D, \lambda) = \frac{C_{sca}}{A_{geo}} \tag{3}$$

where C_{sca} is the effective cross section of scattering, and A_{geo} is the geometric cross section, with most materials assuming a Q_{sca} value between 0 and 1. For very small materials such as SiNWs, whose geometric sizes are below the wavelength of light, it is possible to have scattering efficiencies greater than this, meaning that the scattering cross sections, C_{sca}, is larger than the geometrical area A_{geo} of the object (i.e., the material can scatter light from an area larger than the material itself).

The scattering efficiency (Q_{sca}) of SiNWs can be predicted computationally using Lorentz-Mie theory, and is nonlinearly dependent on the diameter (D) of the SiNW and on the illuminating light's incident angle (ξ), wavelength (λ), and polarization. For this model, SiNWs were assumed to behave optically as infinitely long one-dimensional cylinders, with calculations limited to illuminations perpendicular to the nanowire's long axis ($\xi = 90°$). While some angle dependence has been reported for nanowires,[31] this represents the most general case, and has been shown to be in good agreement with experimentally observed SiNW spectra under darkfield.[4] The effective scattering, Q_{sca} ($\xi = 90°$), was determined for the transversal electric (TE) and transversal magnetic (TM) modes of polarized light using the well-known expression (Figure 5a):[4,17,32]

$$Q_{sca,TE} = \frac{2}{x}\left[|a_0|^2 + 2\sum_{i=1}^{\infty}|a_i|^2\right] \tag{4}$$

$$Q_{sca,TM} = \frac{2}{x}\left[|b_0|^2 + 2\sum_{i=1}^{\infty}|b_i|^2\right] \tag{5}$$

where the expansion coefficients (a_i & b_i) are given by

$$a_i = \frac{\tilde{n}J_i(\tilde{n}x)J_i'(x) - J_i'(\tilde{n}x)J_i(x)}{\tilde{n}J_i(\tilde{n}x)H_i^{(1)'}(x) - J_i'(\tilde{n}x)H_i^{(1)}(x)} \tag{6}$$

$$b_i = \frac{J_i(\tilde{n}x)J_i'(x) - \tilde{n}J_i'(\tilde{n}x)J_i(x)}{J_i(\tilde{n}x)H_i^{(1)'}(x) - \tilde{n}J_i'(\tilde{n}x)H_i^{(1)}(x)} \tag{7}$$

$$\tilde{n} = n + ik \tag{8}$$

$$x = \frac{2\pi}{\lambda}\frac{D}{2} \tag{9}$$

DOI: 10.1021/acs.jpcc.5b10076
J. Phys. Chem. C XXXX, XXX, XXX−XXX

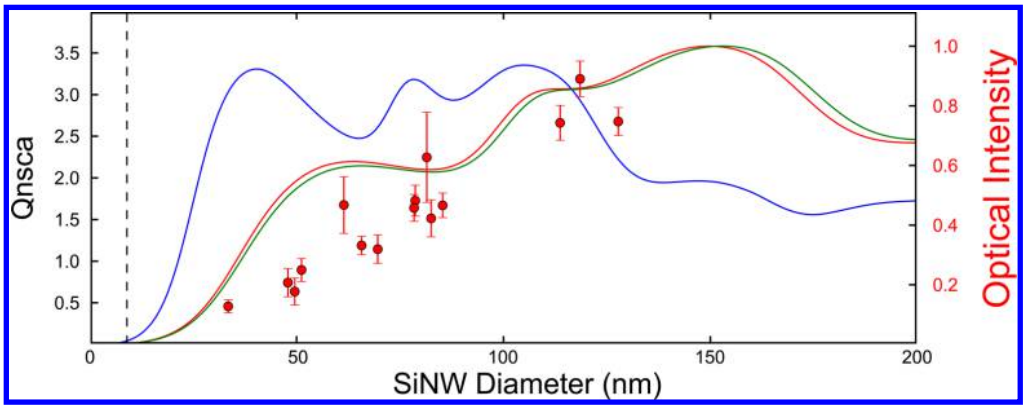

Figure 6. Experimental and predicted scattering efficiencies. Normalized Mie theory predicted scattering efficiencies, Q_{nsca}, of SiNWs using LED illumination in air (blue-line), IPA (red-line), and cytoplasmic fluid (Green-line) as a function of SiNW diameter, D (left axis), superimposed with the relative optical scattering intensity of experimentally measured SiNWs under IPA (Red-Dots, right axis). Horizontal (9 nm marker) suggests the origin of the systematic error present in the optical transform. Sub 150 nm diameter wires show qualitative agreement between predictions and experimentation.

$\tilde{n}$ is the wavelength dependent complex refractive index, J_i is the Bessel function of the first kind of order i, and $H_1^{(i)}$ is the Hankel function of the first kind of order i. For nonpolarized light, the scatter efficiency $Q_{sca,np}$ is given by the expression $Q_{sca,np} = (Q_{sca,TM} + Q_{sca,TE})/2$. Bulk silicon reference values for the wavelength dependent complex refractive index, $\tilde{n}$, were used[33] and quantum confinement effects were ignored for the present study. These are reasonable assumptions for the majority of wires surveyed; however, they may be problematic for smaller wires (d < 5 nm), as SiNW thickness can begin to dominate optical properties.[34] The infinite sums of the Bessel and Hankel functions were approximated analytically to the 10th order, as beyond this no appreciable changes were noted. The scattering efficiencies Q_{sca} were calculated for SiNWs in a number of different media, including air, isopropyl alcohol (IPA), and cellular cytoplasmic fluid (Figure 5b–d). For each medium, a series of different peak scattering efficiencies Q_{sca} were observed, with SiNW scattering efficiencies Q_{sca} depending on both the wavelength (λ) and SiNW diameter. The resulting scattering features were similar for both IPA and cytoplasmic fluid as they have a similar RI; however, these differed from the scattering predicted in air, with IPA and cytoplamic fluid's displaying a distended scattering efficiency in the (λ,d) plane, while air generally displayed sharper scattering peaks between ∼50 nm to ∼150 nm in the visible regime. Additionally, larger scattering efficiencies were predicted at larger diameters under IPA and cytoplasmic fluid than was true in the air case and in each medium, for wavelengths smaller than ∼350 nm, the scattering efficiencies Q_{sca} did not show a strong dependence on SiNW's diameter.

Lorentz-Mie theory offers some insight into SiNW scattering, and can be used to examine the previously mentioned underlying assumption that SiNW scattering intensity scales monotonically with regard to NW diameter. Examining this in the visible regime for a given wavelength, it can be seen that multiple NW diameters show the same predicted scattering efficiency (Figure S5). This suggests that light intensity, at least for a given wavelength, is not a unique metric for determining an SiNW's diameter, and that larger SiNWs do not necessarily scatter light most efficiently. Taken together, this means that single wavelength light does not fulfill our monotonic requirement for using the optical-EM transform.

However, with the exception of lasers, few light sources illuminate over such a narrow range of wavelengths. Therefore, a more reasonable prediction of the scattering intensity observed under DF would take into account both the spectrum of the illuminating lamp and the spectral sensitivity of the detector. To incorporate these factors into our model, we constructed a normalized scattering coefficient, Q_{nsca}, which uses the wavelength dependent intensity of our ring LED source (Figure S6) and the wavelength dependent quantum efficiency of our recording device as weighting coefficients (see Supporting Information for more details). Summing these over the spectral range of the illumination source and normalizing, produced a more reasonable estimate of the expected light scattering, Q_{nsca} (Figure 6, left axis). Using this method, Lorentz-Mie theory predicted scattering efficiencies were compared to the experimentally determined relative optical scattering intensities (Figure 6, right axis), with the maximum observed scattering intensities (<150 nm) scaled to agree with the maximum predicted Q_{nsca} at ∼150 nm (see eq 2). For wires with diameters under 150 nm, the predicted values were seen to be in qualitative agreement with experimentally determined values, with both showing similar scaling and a relatively monotonic increase before ∼150 nm in IPA. This validates our earlier approach, suggesting that the Optical-EM transform is well founded in this size range. However, Lorentz-Mie theory also tended to inflate scattering efficiencies, with a predicted scattering peak at ∼60 nm in IPA, while experimentally observed values show a more modest scaling in this regime. This is likely the result substrate-SiNW interactions and of assuming a fixed angle (ξ = 90°), where a more complete approach would incorporate the setup-dependent darkfield angle, integrating about the circle of illumination (α, Figure 5a); however, this is beyond the scope of the current paper.

Additionally, we noted some limitation in Lorentz-Mie theory's predictive power for larger diameter SiNWs. For larger wires (between ∼260–300 nm), observed scattering intensities significantly out-scaled predicted values (Figure 7) (Scattering intensities normalized to sub 150 nm population). This is the result of an underlying assumption that the wires are embedded in a uniform medium and therefore have minimal interaction with the underlying substrate. For smaller wires whose resonant modes are primarily confined within the wire, this is a reasonable approximation; however, as wires grow larger

DOI: 10.1021/acs.jpcc.5b10076
J. Phys. Chem. C XXXX, XXX, XXX–XXX

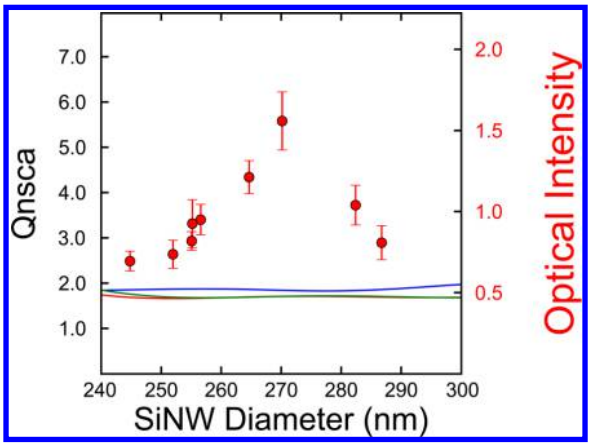

Figure 7. Large diameter SiNW scattering. Mie theory predicted scattering efficiencies, Q_{nsca}, in air (blue-line), IPA (red-line), and cytoplasmic fluid (green-line) (left axis), superimposed with experimentally measured optical scattering intensity of larger diameter SiNWs under IPA (red-dots, right axis). Mie theory fails to recapitulate experimental values for larger SiNWs. (Relative optical intensities scaled to agree with sub 150 nm population.)

these modes can extended noticeably beyond the boundary of the wire, creating some discrepancy between experimentation and theory.[8] This shows, that while Lorentz-Mie scattering was useful for understanding certain trends in optical scattering, its application must be carefully considered for larger wires. This mismatch between theory and experimentation justifies our experimentally based approach for determining the optical-EM transform, rather than using a purely theoretical method to produce the mapping function, as the experimental results do not correspond directly with the theoretical model.

Despite these inconstancies, Lorentz-Mie theory offers some potential insight into understanding SiNW scattering. First, it indicates potential ranges over which the optical-EM transform can perform. For each imaging media, the predicted scattering intensities actually decrease after a certain threshold diameter. This indicates the range over which the optical-EM transform can no longer be safely applied, as past this threshold scattering intensity no longer scales monotonically. Second, Lorentz-Mie theory also indicates the important role that imaging media plays in optical scattering. In air, for instance, predicted scattering efficiencies scale sharply between 0−40 nm before reaching a maximum plateau, and then drop down again near ∼100 nm to a relatively consistent value. While this limits the range of optical-EM transform to between ∼0−40 nm in air, it also suggests that scattering intensity can be used as a very sensitive marker for SiNW diameter in this regime. For IPA and cytosolic fluid, however, a much larger range is predicted, showing a consistent increase in light scattering between ∼0−150 nm. While there is slight dip between ∼54−84 nm, overall this range is relatively monotonic, suggesting that SiNWs fulfill this requirement under real world conditions. The values reported here are specific to the LED ring illuminator used in these experiments, which enabled the simultaneous monitoring of both SiNWs and cellular systems. However, more traditional blackbody irradiators (such as tungsten-cathode lamps) show similar trends, (Figure S7), even predicting an extended monotonic range of up to ∼230 nm in IPA. In this way, Lorentz-Mie theory offers some potential insights into different optical scattering conditions and confirms that our conditions for monotonic scaling are satisfied for wires with diameters under 150 nm in IPA.

Lorentz-Mie theory can also help explain why smaller wires were under-represented in the initial optical-EM transform predictions, leading to a systematic error and the need for a correction factor. By examining the predicted scattering efficiencies of very small wires (<9 nm, Figure 6, dashed line), we can see that these wires showed negligible predicted scattering efficiencies in IPA and cytosolic fluid. This suggests that smaller wires will not be observed appreciably using optical techniques as compared to larger wires, resulting in the previously mentioned population mismatch where smaller wires were under-represented optically compared to the TEM measured values. This threshold appears to occur near ∼10.0 nm, which is in good agreement with the experimentally determined correction factor of 8.9 nm.

Before moving on, we note that the Lorentz-Mie theory presented here represents a rapid analytical approach for exploring SiNW optics and has been shown to be in good agreement for multiple material systems including GaAs[17] and germanium[29] nanowires; however more time-intensive numerical approaches, such as Finite-difference time-domain (FDTD), can also be pursued to provide a more precise theoretical model.[18,35,36] Such approaches offer the benefit of being able to model explicitly substrate nanowire interactions; however, they can also be more time intensive to both implement and run over a large spectral range. As our primary goal in this manuscript was to establish the monotonic range over which the optical-EM transform remains valid, the Lorentz-Mie theory approach offered a valuable tool for rapidly assessing this under multiple conditions; however, those seeking more rigorous theoretical agreement may consider other models.

3.3. Intracellular Force Probes. Using this information, we were able to extend the use of the optical-EM transform to intracellular SiNWs, enabling a more precise determination of forces in optically based SiNW intracellular force probes. Mechanical forces play an important role in regulating cellular behavior, providing cues for intra- and intercellular signaling.[37,38] SiNW force probes are a promising class of material for examining these processes, as they can be distributed in a drug-like fashion, are relatively easy to implement, offering the potential for long-term continuous multiplexed force detection.[25] Additionally, unlike other intracellular force probing mechanisms, such as optical tweezers,[39] and fluorescent molecular probes,[40,41] SiNW force probes are resistant to fluorescent bleaching[42] and localized photothermal heating, both of which can limit experimental time-scales.[43]

While the reported probes can precisely predict relative force changes,[25] their ability to determine absolute forces was hampered by the accuracy the SiNW diameter measurement, as the force probes reported in this study are extremely sensitive to NW diameters, with forces scaling to the fourth power with respect to SiNW diameter. One way to resolve this issue is using electron microscopy studies in conjunction with these probes; however, such studies are time-consuming, and are difficult to link to specific probes within individual cells. The optical-EM transform allows a route to circumvent this requirement, as electron microscopy studies can be performed in an ensemble fashion, using wires prepared from the same sample, rather than the specific force probe itself, while still allowing a precise determination of the NW's diameter.

DOI: 10.1021/acs.jpcc.5b10076
J. Phys. Chem. C XXXX, XXX, XXX−XXX

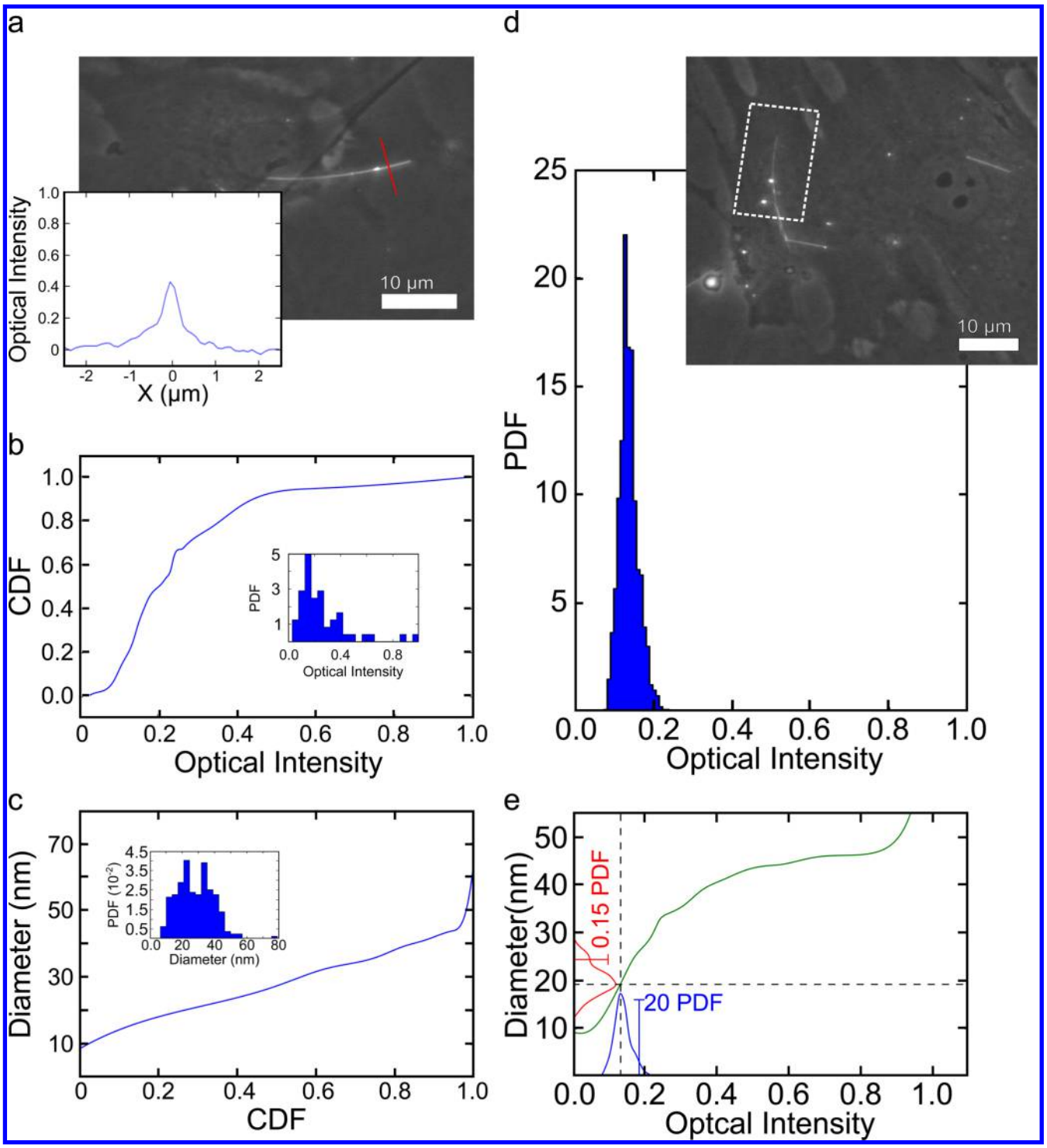

Figure 8. (a) Example SEPC image of a SiNW in the cellular microenvironment with the corresponding line scan taken over the region indicated in red. (b) Cumulative distribution function (CDF) of the ensemble SiNW optical scattering intensity, with the associated population distribution (inset). (c) Inverse CDF of the ensemble SiNW diameters as measured by TEM, with associated population distribution (inset). (d) Measured optical scattering intensity of the kinked SiNW force probe, with associated SEPC micrograph. Scattering intensities collected over the highlighted region of the sensor's arm. (e) Optical-EM transform to determine the SiNW's diameter (green), showing the superimposed intensity distribution (blue, scaled as a PDF in blue), and the resulting uncertainty in SiNW diameter (superimposed in red, scaled as a PDF in red, precorrection factor).

To test these probes, human aortic smooth muscle cells (HASMCs) were selected as a model cell line, as contraction can be easily induced using the hormone angiotension II (Video S1). Kinked SiNW force probes were introduced 72 h before force measurements, allowing cells time to internalize the wires, and with samples monitored using scatter enhanced phase contrast (SEPC).[25] By monitoring the shape of SiNW deformation, we were able to extract force information from the probes, with nanowire bending modeled using the Euler–Bernoulli equations for the deflection of a simple beam supported under an asymmetric point load (Figure 2):

DOI: 10.1021/acs.jpcc.5b10076
J. Phys. Chem. C XXXX, XXX, XXX−XXX

$$dY(x) = \begin{cases} \dfrac{Pbx(L^2 - b^2 - x^2)}{6LEI} & \mathbf{0 \le x \le L - b} \\ \dfrac{Pbx(L^2 - b^2 - x^2)}{6LEI} + \dfrac{P(x - L + b)^3}{6EI} & L - b < x \le L \end{cases} \tag{10}$$

where P is the force of the load, L is the length of the wire, b is the distance of the point-load from the wire tip, and E and I are the elastic Young's modulus and the beams' cross sectional moment of inertia respectively ($\mathbf{I} = (5\sqrt{3})/(144)D^4$). The KSiNWs growth direction was primarily ⟨112⟩ and with a Young's modulus of 169 GPa.[44,45] While cytoskeletal imaging suggests that the force is distributed over the nanowire, a point load acts as a good approximation for the total sum of forces and accounts for asymmetries in the force distribution.[25] The point load location b was determined on a frame-by-frame basis using the relationship:

$$b = \sqrt{L^2 - 3x_{max}^2} \tag{11}$$

where x_{max} is the x coordinate of maximum deflection (Figure 2). x_{max} was determined using a 10-point moving average to smooth the raw SiNW coordiantes.[46] Fitting for the load parameter P, forces were measured using a least-squares regression of eq 10.

To precisely measure intracellular forces, the probe's diameter was determined using the optical-EM transform to convert optical intensity measurements into diameter information. The intracellular optical-EM transform was constructed for force probes in an analogous fashion to those previously mentioned (Figure 8), with the ensemble optical measurements obtained using an internal control model (Figure 8a) (i.e., other wires present within the sample solution), mitigating the effects of cellular exposure on the optical scattering profile. Control samples were imaged immediately after force measurements, using the same incident light intensity and exposure conditions. The intracellular optical-EM transform was then applied to the optical scattering recorded from the individual probe, yielding a mode diameter prediction of 27.7 ± 3.2 nm (Figure S8) (error given as the standard deviation of the transformed scattering intensity measurements). Using this diameter, the Euler–Bernoulli equations were found to be in good agreement with experimental determined optical deformations (Figure 9b), with HASMCs showing optimal contraction times around ∼30 min, and maximum predicted force peaks on the order of 171 pN (Figure 9c).

The use of the optical-EM transform enabled an estimate of uncertainty present in these force measurements. Using the distribution of possible NW diameters, an example frame (Figure 9b) was refit using the modified SiNW diameter and the respective values for the cross sectional moment of inertia **I**. This yielded a range of possible force measurements that could be observed (Figure 10), estimating a standard deviation of ±102 pN, or an error of ∼59%. While this is larger than the ∼10% error values reported using magnetic tweezers,[47] this represents a substantial decrease in the error associated with this type of measurement using the base force probe's diameter distribution. Although the standard deviation of the default growth sample was only ∼10 nm, this corresponds to standard deviation in force measurements of ∼12 672 pN (Figure S9). As a result, the optical-EM transform yields a more than 100-fold increase in the accuracy of these force measurements, marking this a substantial improvement, and demonstrating the power of the optical-EM transform in addressing practical biomaterial applications.

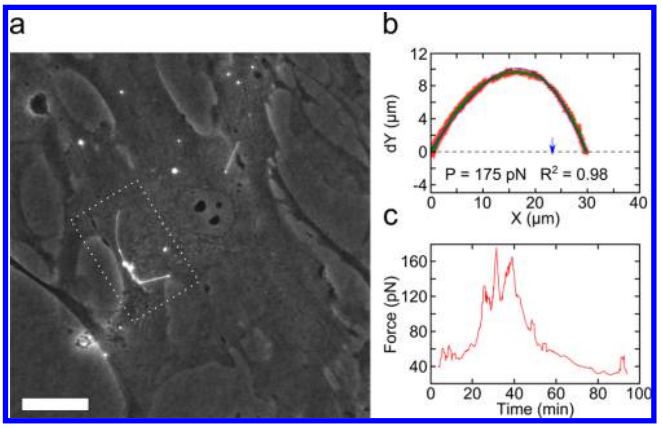

Figure 9. SiNWs as Intracellular Force Probes. (a) SEPC micrograph of a kinked SiNW force probe internalized in a HASMC, with schematic diagram showing SiNW force model (inset). (b) Single frame example of SiNW force fitting data. (Red, SiNW coordinates; green, averaged center; blue, force fitting data; blue arrow, position of force load). (c) Intracellular force over time, during angiotensin-induced muscle contraction.

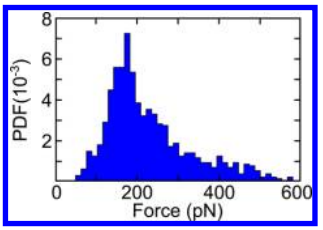

Figure 10. Uncertainty in force measurements. Uncertainty in force measurements determined by fitting an example frame using the distribution of possible SiNW diameters determined by the optical-EM transform (mode: 171 pN, mean: 230 pN, standard deviation: 104 pN).

4. CONCLUSIONS

A scalable method to optically determine SiNW diameters based on their scattering intensity and ensemble diameter measurements has been presented. This method allows for the determination of a sample's diameter within an accuracy of a few nanometers, providing diffraction-limited information, with an associated error of less than 10%. Although the models presented here are specific to silicon-based devices, we believe that this method could be easily implemented in other nanomaterials, such as germanium and silver nanowires, and that Lorentz-Mie theory offers a powerful tool for understanding how light scattering scales in these systems as a first-approximation. By using this method for in situ intracellular optical force probes, we have shown how this technique can help provide resolution-limited information in situations where it might otherwise be challenging to obtain directly, and how such techniques can be important for studying the bionano interface. Finally, we believe that this method has substantial promise for use with SiNW based optoelectronic devices such as sensors, photovoltaics, and photodetectors. By enabling a quick determination of an NW's diameter, this work could be a substantial boon for large-scale quality assurance and device calibration efforts.

DOI: 10.1021/acs.jpcc.5b10076
J. Phys. Chem. C XXXX, XXX, XXX−XXX

■ ASSOCIATED CONTENT

Supporting Information

The Supporting Information is available free of charge on the ACS Publications Web site. The PDF Includes Additionally, a is included. The Supporting Information is available free of charge on the ACS Publications website at DOI: 10.1021/acs.jpcc.5b10076.

Additional information on computation, error correction, how the correlative microscopy was performed, and how values of Q_{nsca} were determined (PDF)

Complete video of the internalized SiNW force probe with the corresponding frame fitting data and force measurements (AVI)

■ AUTHOR INFORMATION

Corresponding Author

*E-mail: btian@uchicago.edu (B.T.).

Notes

The authors declare no competing financial interest.

■ ACKNOWLEDGMENTS

We would like to thank J. Jumper for his technical advice in modeling the optical-EM transform, and E. Malachosky for assisting in LED spectral measurements. This work is supported by Air Force Office of Scientific Research (AFOSR FA9550-14-1-0175), National Science Foundation (NSF CAREER, DMR-1254637; NSF MRSEC, DMR-0820054), Searle Scholars Foundation, and the University of Chicago start-up fund.

■ REFERENCES

(1) Street, R. a; Wong, W. S.; Paulson, C. Analytic Model for Diffuse Reflectivity of Silicon Nanowire Mats. *Nano Lett.* **2009**, *9* (10), 3494−3497.

(2) Tsakalakos, L. Strong Broadband Optical Absorption in Silicon Nanowire Films. *J. Nanophotonics* **2007**, *1* (1), 013552.

(3) Muskens, O. L.; Diedenhofen, S. L.; van Weert, M. H. M.; Borgström, M. T.; Bakkers, E. P. a M.; Rivas, J. G. Epitaxial Growth of Aligned Semiconductor Nanowire Metamaterials for Photonic Applications. *Adv. Funct. Mater.* **2008**, *18* (7), 1039−1046.

(4) Brönstrup, G.; Jahr, N.; Leiterer, C.; Csáki, A.; Fritzsche, W.; Christiansen, S. Optical Properties of Individual Silicon Nanowires for Photonic Devices. *ACS Nano* **2010**, *4* (12), 7113−7122.

(5) Priolo, F.; Gregorkiewicz, T.; Galli, M.; Krauss, T. F. Silicon Nanostructures for Photonics and Photovoltaics. *Nat. Nanotechnol.* **2014**, *9* (1), 19−32.

(6) Kelzenberg, M. D.; Turner-Evans, D. B.; Kayes, B. M.; Filler, M. a; Putnam, M. C.; Lewis, N. S.; Atwater, H. a. Photovoltaic Measurements in Single-Nanowire Silicon Solar Cells. *Nano Lett.* **2008**, *8* (2), 710−714.

(7) Zhang, X.; Pinion, C. W.; Christesen, J. D.; Flynn, C. J.; Celano, T. a.; Cahoon, J. F. Horizontal Silicon Nanowires with Radial P−n Junctions: A Platform for Unconventional Solar Cells. *J. Phys. Chem. Lett.* **2013**, *4* (12), 2002−2009.

(8) Cao, L.; Fan, P.; Vasudev, A. P.; White, J. S.; Yu, Z.; Cai, W.; Schuller, J. a.; Fan, S.; Brongersma, M. L. Semiconductor Nanowire Optical Antenna Solar Absorbers. *Nano Lett.* **2010**, *10* (2), 439−445.

(9) Tian, B.; Zheng, X.; Kempa, T. J.; Fang, Y.; Yu, N.; Yu, G.; Huang, J.; Lieber, C. M. Coaxial Silicon Nanowires as Solar Cells and Nanoelectronic Power Sources. *Nature* **2007**, *449* (7164), 885−889.

(10) YAMADA, H.; CHU, T.; ISHIDA, S.; ARAKAWA, Y. Si Photonic Wire Waveguide Devices. *IEICE Trans. Electron.* **2007**, *E90-C* (1), 59−64.

(11) Wang, H.; Fan, P.-H.; Tong, B.; Dong, Y.-P.; Ou, X.-M.; Li, F.; Zhang, X.-H. Hydrogen-Terminated Si Nanowires as Label-Free Colorimetric Sensors in the Ultrasensitive and Highly Selective Detection of Fluoride Anions in Pure Water Phase. *Adv. Funct. Mater.* **2015**, *25* (10), 1506−1510.

(12) Zhang, A.; You, S.; Soci, C.; Liu, Y.; Wang, D.; Lo, Y.-H. Silicon Nanowire Detectors Showing Phototransistive Gain. *Appl. Phys. Lett.* **2008**, *93* (12), 121110.

(13) Yang, C.; Barrelet, C. J.; Capasso, F.; Lieber, C. M. Single P-Type/Intrinsic/n-Type Silicon Nanowires as Nanoscale Avalanche Photodetectors. *Nano Lett.* **2006**, *6* (12), 2929−2934.

(14) Lee, S.-H.; Baek, C.-K.; Park, S.; Kim, D.-W.; Sohn, D. K.; Lee, J.-S.; Kim, D. M.; Jeong, Y.-H. Characterization of Channel-Diameter-Dependent Low-Frequency Noise in Silicon Nanowire Field-Effect Transistors. *IEEE Electron Device Lett.* **2012**, *33* (10), 1348−1350.

(15) Singh, N.; Lim, F. Y.; Fang, W. W.; Rustagi, S. C.; Bera, L. K.; Agarwal, A.; Tung, C. H.; Hoe, K. M.; Omampuliyur, S. R.; Tripathi, D. et al. Ultra-Narrow Silicon Nanowire Gate-All-Around CMOS Devices: Impact of Diameter, Channel-Orientation and Low Temperature on Device Performance. In *2006 International Electron Devices Meeting*; IEEE, 2006; pp 1−4.

(16) Kempa, T. J.; Cahoon, J. F.; Kim, S.-K.; Day, R. W.; Bell, D. C.; Park, H.-G.; Lieber, C. M. Coaxial Multishell Nanowires with High-Quality Electronic Interfaces and Tunable Optical Cavities for Ultrathin Photovoltaics. *Proc. Natl. Acad. Sci. U. S. A.* **2012**, *109* (5), 1407−1412.

(17) Brönstrup, G.; Leiterer, C.; Jahr, N.; Gutsche, C.; Lysov, A.; Regolin, I.; Prost, W.; Tegude, F. J.; Fritzsche, W.; Christiansen, S. A Precise Optical Determination of Nanoscale Diameters of Semiconductor Nanowires. *Nanotechnology* **2011**, *22* (38), 385201.

(18) Cao, L.; Fan, P.; Barnard, E. S.; Brown, A. M.; Brongersma, M. L. Tuning the Color of Silicon Nanostructures. *Nano Lett.* **2010**, *10* (7), 2649−2654.

(19) Heurlin, M.; Anttu, N.; Camus, C.; Samuelson, L.; Borgström, M. T. In Situ Characterization of Nanowire Dimensions and Growth Dynamics by Optical Reflectance. *Nano Lett.* **2015**, *15* (5), 3597−3602.

(20) Jacques, S. L. Optical Properties of Biological Tissues: A Review. *Phys. Med. Biol.* **2013**, *58* (11), R37−R61.

(21) Zhang, W.; Tong, L.; Yang, C. Cellular Binding and Internalization of Functionalized Silicon Nanowires. *Nano Lett.* **2012**, *12* (2), 1002−1006.

(22) Zimmerman, J.; Parameswaran, R.; Tian, B. Nanoscale Semiconductor Devices as New Biomaterials. *Biomater. Sci.* **2014**, *2* (5), 619.

(23) Tian, B.; Cohen-Karni, T.; Qing, Q.; Duan, X.; Xie, P.; Lieber, C. M. Three-Dimensional, Flexible Nanoscale Field-Effect Transistors as Localized Bioprobes. *Science* **2010**, *329* (5993), 830−834.

(24) Chiappini, C.; De Rosa, E.; Martinez, J. O.; Liu, X.; Steele, J.; Stevens, M. M.; Tasciotti, E. Biodegradable Silicon Nanoneedles Delivering Nucleic Acids Intracellularly Induce Localized in Vivo Neovascularization. *Nat. Mater.* **2015**, *14* (5), 532−539.

(25) Zimmerman, J. F.; Murray, G. F.; Wang, Y.; Jumper, J. M.; Austin, J. R.; Tian, B. Free-Standing Kinked Silicon Nanowires for Probing Inter- and Intracellular Force Dynamics. *Nano Lett.* **2015**, *15* (8), 5492−5498.

(26) Razi, M.; Tooze, S. a. Chapter 17. Correlative Light and Electron Microscopy. In *Methods in Enzymology*; Elsevier Inc., 2009; Vol. *452*, pp 261−275.

(27) Tian, B.; Xie, P.; Kempa, T. J.; Bell, D. C.; Lieber, C. M. Single-Crystalline Kinked Semiconductor Nanowire Superstructures. *Nat. Nanotechnol.* **2009**, *4* (12), 824−829.

(28) Venkatapathi, M.; Kumar Tiwari, A. Radiative and Non-Radiative Effects of a Substrate on Localized Plasmon Resonance of Particles. *J. Appl. Phys.* **2012**, *112* (1), 013529.

(29) Cao, L.; White, J. S.; Park, J.-S.; Schuller, J. a; Clemens, B. M.; Brongersma, M. L. Engineering Light Absorption in Semiconductor Nanowire Devices. *Nat. Mater.* **2009**, *8* (8), 643−647.

(30) Phillips, K. G.; Jacques, S. L.; McCarty, O. J. T. Measurement of Single Cell Refractive Index, Dry Mass, Volume, and Density Using a Transillumination Microscope. *Phys. Rev. Lett.* **2012**, *109* (11), 118105.

DOI: 10.1021/acs.jpcc.5b10076
J. Phys. Chem. C XXXX, XXX, XXX−XXX

(31) Knight, M. W.; Fan, J.; Capasso, F.; Halas, N. J. Influence of Excitation and Collection Geometry on the Dark Field Spectra of Individual Plasmonic Nanostructures. *Opt. Express* **2010**, *18* (3), 2579.
(32) Bohren, C. F.; Huffman, D. R. *Absorption and Scattering of Light by Small Particles*; Bohren, C. F., Huffman, D. R., Eds.; Wiley-VCH Verlag GmbH: Weinheim, Germany, 1998.
(33) Palik, E. D. *Handbook of Optical Constants of Solids*; Palik, E. D., Ed.; Academic Press: New York, 1989; Vol. 3.
(34) Ma, D. D. D. Small-Diameter Silicon Nanowire Surfaces. *Science (Washington, DC, U. S.)* **2003**, *299* (5614), 1874−1877.
(35) Myroshnychenko, V.; Rodríguez-Fernández, J.; Pastoriza-Santos, I.; Funston, A. M.; Novo, C.; Mulvaney, P.; Liz-Marzán, L. M.; García de Abajo, F. J. Modelling the Optical Response of Gold Nanoparticles. *Chem. Soc. Rev.* **2008**, *37* (9), 1792.
(36) Gallinet, B.; Butet, J.; Martin, O. J. F. Numerical Methods for Nanophotonics: Standard Problems and Future Challenges. *Laser Photon. Rev.* **2015**, *9*, 6, p 57710.1002/lpor.201500122.
(37) Wang, N.; Butler, J. P.; Ingber, D. E. Mechanotransduction across the Cell Surface and through the Cytoskeleton. *Science* **1993**, *260*, 1124−1127.
(38) Fletcher, D. a; Mullins, R. D. Cell Mechanics and the Cytoskeleton. *Nature* **2010**, *463*, 485−492.
(39) Oddershede, L. B. Force Probing of Individual Molecules inside the Living Cell Is Now a Reality. *Nat. Chem. Biol.* **2012**, *8* (11), 879−886.
(40) Grashoff, C.; Hoffman, B. D.; Brenner, M. D.; Zhou, R.; Parsons, M.; Yang, M. T.; McLean, M. a; Sligar, S. G.; Chen, C. S.; Ha, T.; et al. Measuring Mechanical Tension across Vinculin Reveals Regulation of Focal Adhesion Dynamics. *Nature* **2010**, *466* (7303), 263−266.
(41) Wang, X.; Ha, T. Defining Single Molecular Forces Required to Activate Integrin and Notch Signaling. *Science* **2013**, *340* (May), 991−994.
(42) Marawske, S.; Dörr, D.; Schmitz, D.; Koslowski, A.; Lu, Y.; Ritter, H.; Thiel, W.; Seidel, C. a M.; Kühnemuth, R. Fluorophores as Optical Sensors for Local Forces. *ChemPhysChem* **2009**, *10*, 2041−2048.
(43) Neuman, K. C.; Chadd, E. H.; Liou, G. F.; Bergman, K.; Block, S. M. Characterization of Photodamage to Escherichia Coli in Optical Traps. *Biophys. J.* **1999**, *77* (5), 2856−2863.
(44) Sohn, Y.-S.; Park, J.; Yoon, G.; Song, J.; Jee, S.-W.; Lee, J.-H.; Na, S.; Kwon, T.; Eom, K. Mechanical Properties of Silicon Nanowires. *Nanoscale Res. Lett.* **2010**, *5* (1), 211−216.
(45) San Paulo, a.; Bokor, J.; Howe, R. T.; He, R.; Yang, P.; Gao, D.; Carraro, C.; Maboudian, R. Mechanical Elasticity of Single and Double Clamped Silicon Nanobeams Fabricated by the Vapor-Liquid-Solid Method. *Appl. Phys. Lett.* **2005**, *87* (5), 053111.
(46) Qin, Q.; Zhu, Y. Static Friction between Silicon Nanowires and Elastomeric Substrates. *ACS Nano* **2011**, *5* (9), 7404−7410.
(47) te Velthuis, A. J. W.; Kerssemakers, J. W. J.; Lipfert, J.; Dekker, N. H. Quantitative Guidelines for Force Calibration through Spectral Analysis of Magnetic Tweezers Data. *Biophys. J.* **2010**, *99* (4), 1292−1302.

DOI: 10.1021/acs.jpcc.5b10076
J. Phys. Chem. C XXXX, XXX, XXX−XXX